Electronic Supplementary Material (ESI) for Materials Chemistry Frontiers.

Supporting Information

Fusing rigid planar units to engineer twisting molecules as dual-state emitters

Yuanye Yin,[a] Aixiang Ding,[b,*] Longmei Yang, [a] Lin Kong,[a] and Jiaxiang Yang [a,*]

[a]*College of Chemistry and Chemical Engineering, Key Laboratory of Structure and Functional Regulation of Hybrid Materials (Anhui University), Ministry of Education, Photoelectric Conversion Energy Materials and Devices Key Laboratory of Anhui Province, Anhui University, Hefei, 230061, PR China .*

[b]*College of Chemistry and Chemical Engineering, Xinyang Normal University, Xinyang, 464000, PR China.*

**Corresponding authors. E-mails: J.X.Y.* jxyang@ahu.edu.cn*; A.X.D.* dax@xynu.edu.cn

1. Materials and instruments

All chemicals and reagents are analytical grade products purchased from the market, which are not purified when used. Melting points were determined by an Polarizing micro melting point meter. FT-IR spectroscopy was obtained on the Thermo Fisher-Summit Pro spectrometer (4000–400 cm^{-1} KBr pellet). The ^{1}H NMR (400 MHz) and ^{13}C NMR (100 MHz) spectra were obtained on a Bruker Avance II DMX 400 spectrometer with $CDCl_3$ as the solvent. High-resolution mass spectra (HR-MS) data were obtained by using a triple quadrupole mass spectrometer equipped with electrospray source ion (ESI). The UV-vis absorption spectra were recorded using a UV 3600 spectrophotometer from Japan Shimadzu Corporation with samples in solution and a quartz cuvette (path length 1 cm), and the fluorescence spectra were obtained on a Hitachi FL-7100 (Hitachi high technologies corporation Tokyo Japan). The absolute photoluminescence quantum yield in the solid state was measured on a HORIBA FluoroMax-4 spectrofluorometer using an integrating sphere (HORIBA Scientific, F-3092 integrating sphere). The powder X-ray diffraction (PXRD) patterns were recorded on an MXP18AHF diffractometer using Cu-Ka radiation (λ = 1.54056 Å in the 2θ range from 2° to 60°. The X-ray diffraction measurement of a single crystal was performed on a Bruker SMART II CCD area detector using graphite-monochromated Cu-Ka radiation.

2. Compound synthesis

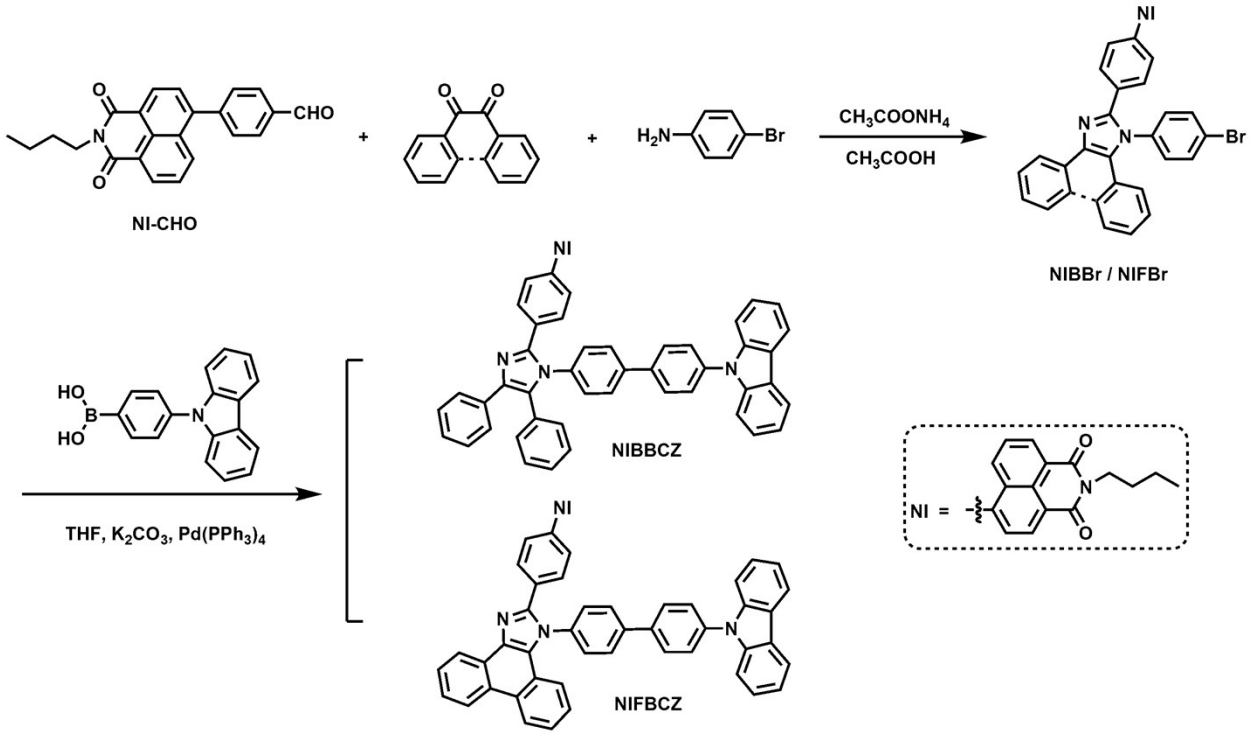

Scheme 1. Synthesis of **NIBBCZ** and **NIFBCZ**.

*2.1 Synthesis of **NIBBr** and **NIFBr***

NI-CHO was synthesized according to the reported literature.[S1]

At room temperature, benzil/phenanthrenequinone (1.12 mmol) and 4-bromoaniline (0.15 g, 1.68 mmol) were added to 25 mL glacial acetic acid in batches and reacted for 20 min. Then **NI-CHO** (0.40 g, 1.12 mmol) and ammonium acetate (0.43 g, 5.60 mmol) were added to the mixed solution and refluxed at 110 °C for 4.0 h. As the system cooled to room temperature, the reaction solution was poured into water (100 mL), the pH was adjusted to neutral with 40% NaOH solution. The precipitated residue was purified by a silica gel column chromatography with ethyl acetate/petroleum ether (1:3 v/v) as the eluent.

Compound **NIBBr**: yellow-green solid, yield 59%. ^{1}H NMR ($CDCl_3$, 400 MHz, ppm) δ: 0.96-1.00 (t, J = 7.36 Hz, 3H), 1.41-1.48 (m, 2H), 1.69-1.77 (m, 2H), 4.18-4.22 (t, J = 7.60 Hz, 2H),

6.99-7.01 (d, *J* = 8.64 Hz, 2H), 7.14-7.24 (m, 4H), 7.26-7.31 (m, 4H), 7.42-7.45 (m, 4H), 7.59-7.62 (m, 4H), 7.67-7.72 (m, 2H), 8.22-8.24 (d, *J* = 8.52 Hz, 1H), 8.61-8.63 (d, *J* = 7.52 Hz, 2H). ^{13}C NMR ($CDCl_3$, 100 MHz, ppm) δ: 13.95, 20.49, 30.32, 40.39, 122.09, 122.65, 123.08, 127.06, 127.45, 127.89, 128.35, 128.74, 129.15, 130.01, 130.23, 130.54, 130.82, 131.20, 131.32, 132.64, 134.1

Compound **NIFBr**: yellow-green solid, yield 85%. ^{1}H NMR ($CDCl_3$, 400 MHz, ppm) δ: 0.97-1.00 (t, *J* = 7.40 Hz, 3H), 1.41-1.51 (m, 2H), 1.69-1.77 (m, 2H), 4.17-4.21 (t, *J* = 7.60 Hz, 2H), 7.20-7.22 (m, 1H), 7.30-7.34 (m, 1H), 7.44-7.49 (m, 4H), 7.51-7.55 (t, *J* = 8.36 Hz, 3H), 7.63-7.69 (m, 3H), 7.72-7.79 (m, 5H), 8.18-8.20 (d, *J* = 8.52 Hz, 1H), 8.58-8.60 (d, *J* = 7.52 Hz, 2H), 8.67-8.69 (d, *J* = 8.32 Hz, 1H), 8.74-8.76 (d, *J* = 8.28 Hz, 1H), 8.85-8.87 (d, *J* = 7.92 Hz, 1H). ^{13}C NMR ($CDCl_3$, 100 MHz, ppm) δ: 13.97, 20.51, 30.32, 40.39, 120.76, 122.14, 122.81, 123.04, 123.25, 124.19, 124.37, 125.35, 126.01, 127.06, 127.53, 127.84, 128.29, 128.44, 128.72, 129.63, 130.08, 130.56, 130.74, 130.85, 131.27, 132.33, 133.71, 137.84, 139.49, 145.81, 150.08, 164.12, 164.31.0, 136.20, 138.94, 146.08, 146.16, 164.20, 164.39.

*2.2 Synthesis of **NIBBCZ** and **NIFBCZ***

At room temperature, **NIBBr**/**NIFBr** (0.30 mmol) and 4-(9H-carbazole-9-yl) phenylboronic acid (0.6 mmol) was added to THF solution (30 mL), followed by K_2CO_3 aqueous solution (10 mL, 2 mol/L) and $Pd(PPh_3)_4$ (2 mg). The resulted solution was refluxed for 12 h under N_2 balloon and then cooled to room temperature. The solution was and extracted with CH_2Cl_2 (3 × 30 mL). The organic layers were dried over anhydrous Na_2SO_4 and filtrated. The filtrate was concentrated and the residue was purified by a silica gel column chromatography with CH_2Cl_2 / petroleum ether (2:1 v/v) as the eluent.

Compound **NIBBCZ**: light green solid, yield 78%. FT-IR (KBr, cm^{-1}): 3049, 2949, 2862, 2348, 1914, 1694, 1648, 1594, 1494, 1453, 1360, 1233, 1174, 1067, 1013, 960, 847, 779, 753, 693, 620. ^1H NMR ($CDCl_3$, 400 MHz, ppm) δ: 0.96-1.00 (t, *J* = 7.40 Hz, 3H), 1.41-1.50 (m, 2H), 1.69-1.77 (m, 2H), 4.18-4.21 (t, *J* = 7.64 Hz, 2H), 7.21-7.24 (m, 2H), 7.26-7.31 (m, 10H), 7.38-7.45 (m, 6H), 7.63-7.72 (m, 10H), 7.80-7.82 (d, *J* = 8.56 Hz, 2H), 8.13-8.15 (d, *J* = 7.72 Hz, 2H), 8.25-8.27 (m, 1H), 8.60-8.63 (m, 2H). ^{13}C NMR ($CDCl_3$, 100 MHz, ppm) δ: 13.97, 20.51, 30.33, 40.39, 109.75, 120.26, 120.52, 122.04, 123.07, 123.61, 126.13, 127.02, 127.52, 127.83, 128.38, 128.52, 128.68, 128.79, 129.07, 129.17, 129.97, 130.57, 130.80, 130.89, 131.30, 131.52, 132.52, 134.37, 136.62, 137.67, 138.46, 138.78, 138.95, 140.25, 140.79, 146.19, 146.26, 164.18, 164.37. ESI-MS: m/z ($[M+H]^+$) calcd: 865.3543, found = 865.3558. Melting point = 347 - 350 ℃.

Compound **NIFBCZ**: yellow-green solid, yield 84%. FT-IR (KBr, cm^{-1}): 3055, 2949, 2869, 2354, 1914, 1701, 1661, 1594, 1500, 1447, 1353, 1227, 1174, 1074, 1000, 953, 833, 786, 753, 713, 673, 620, 539. ^1H NMR ($CDCl_3$, 400 MHz, ppm) δ: 0.96-1.00 (t, *J* = 7.20 Hz, 3H), 1.42-1.50 (m, 2H), 1.70-1.77 (m, 2H), 4.18-4.21 (t, *J* = 7.00 Hz, 2H), 7.30-7.38 (m, 4H), 7.42-7.49 (m, 6H), 7.54-7.57 (t, *J* = 7.24 Hz, 1H), 7.67-7.79 (m, 8H), 7.85-7.87 (d, *J* = 7.92 Hz, 2H), 7.99-8.01 (d, *J* = 7.72 Hz, 4H), 8.16-8.18 (d, *J* = 7.72 Hz, 2H), 8.23-8.25 (d, *J* = 8.52 Hz, 1H), 8.60-8.62 (d, *J* = 7.40 Hz, 2H), 8.73-8.75 (d, *J* = 8.12 Hz, 2H), 8.80-8.82 (d, *J* = 8.24 Hz, 1H), 8.91-8.93 (d, *J* = 7.92 Hz, 1H). ^{13}C NMR ($CDCl_3$, 100 MHz, ppm) δ: 13.97, 20.51, 30.32, 40.40, 109.78, 120.35, 120.57, 121.01, 122.12, 122.86, 123.08, 123.31, 123.68, 124.36, 125.30, 125.97, 126.19, 126.57, 127.03, 127.25, 127.54, 127.70, 127.83, 128.57, 128.80, 129.65, 129.79, 130.05, 130.75, 131.28, 132.39, 137.84, 138.03, 138.15, 138.26, 139.37, 140.79, 141.77, 145.96, 150.19, 164.14, 164.33. ESI-MS: m/z ($[M+H]^+$) calcd: 863.3386, found = 863.3413. Melting point = 330 - 332 ℃.

3. General procedure for photophysical characterizations and optical sensing

The luminophores **NIFBCZ** and **NIBBCZ** were dissolved in organic solvents to prepare 10 mM stock solution. The final sample solutions for the measurements (10 μM) in different solvents were obtained by diluting the stock solution in their corresponding solvents, which were then used for measuring UV–vis absorptions and fluorescence at room temperature.

4. Solid state UV-vis and fluorescence spectra

Solid powders were loaded into a quartz plate with a circular groove (diameter 10 mm × depth 0.5 mm). The quartz plate was covered with a quartz slide and then used for solid-state UV-vis and fluorescence measurements.

5. Single X-ray Crystallography

Single crystals of **NIFBCZ** and **NIBBCZ** were grown by slow solvent evaporation crystallization method using DCM as a solvent. Needle-like single crystals in yellow color were obtained and used for SXRD. The corresponding X-ray crystallography data were collected on a Siemens Smart 1000 CCD diffractometer. To request the CCDC numbers of the two DSEgens, the SXRD information was submitted to "The Cambridge Crystallographic Data Centre (CCDC)" at http://www.ccdc.cam.ac.uk/. The SXRD data can be requested free of charge from The Cambridge Crystallographic Data Centre via www.ccdc.cam.ac.uk/data_request/cif.

6. Theoretical calculations

The geometries of **NIFBCZ**, **NIBBCZ**, and PA were optimized in the gas phase on the basis of DFT using the Gaussian 09 package. The RB3LYP/6-31G* basis set was used for used for all the calculations. The electronic cloud distribution and the energies of the LUMO and the HOMO

levels were used for the understanding of the dual-state photophysical properties and for the investigation of the PET mechanism in the PA sensing.

7. Detection of PA

The fluorescence titration of PA was performed by adding different amounts of PA into the working solutions of **NIFBCZ** and **NIBBCZ** in THF at room temperature. The LoD was determined according to the 3-sigma criterion.[52] The Stern-Volmer equation shown as below was used for the determination of the quenching constant (Ksv): $I_0/I = Ksv[Q] + 1$, where I_0 denotes the initial fluorescence intensity, I denotes the fluorescence intensity in the presence of PA, and [Q] denotes the PA concentration.

Caution! PA and other NACs used in the present study are highly explosive and should be handled only in small quantities with the best precautions.

8. Detection of trace water in organic solvents

The stock solutions of **NIFBCZ** and **NIBBCZ** in anhydrous THF were diluted to the 10 μM working solution with THF solvent. Deionized water was added into the THF solutions to afford solutions with different water contents. Then, the fluorescent titration was carried out by recording the fluorescence spectra at various water contents.

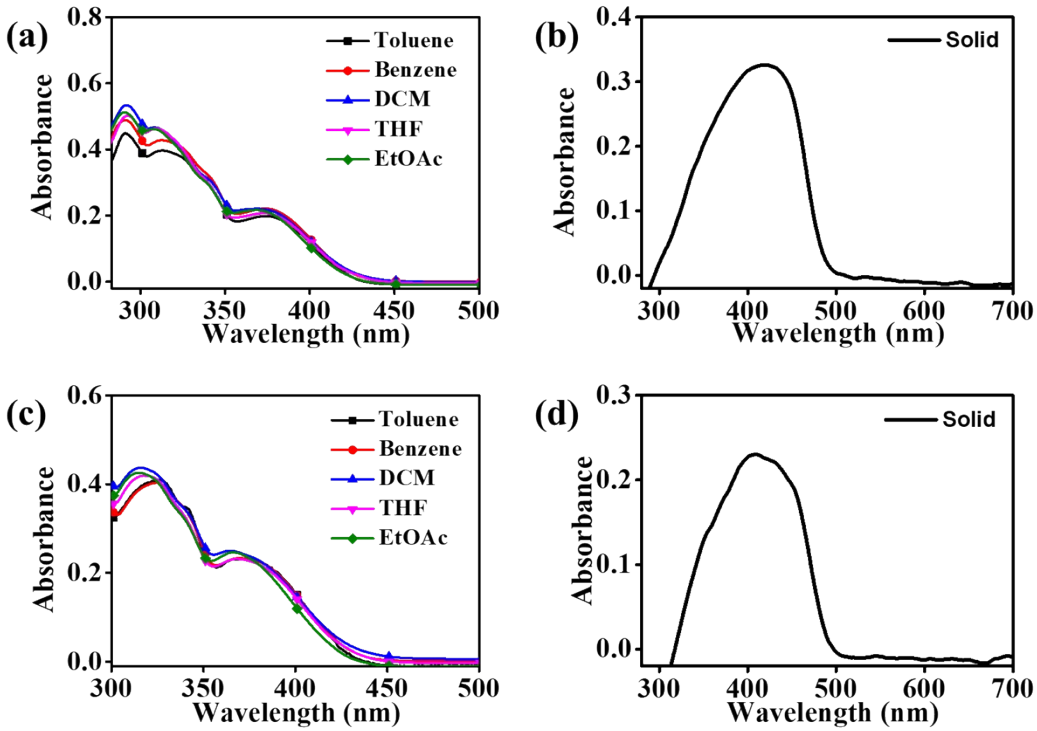

Fig. S1 UV-vis spectra of **NIBBCZ** in (a) different solutions and (b) the solid state and **NIFBCZ** in (c) different solutions and (d) the solid state. Solution concentration is 10 μM, testing temperature is 25 °C.

Table S1 Photophysical properties of **NIBBCZ** and **NIFBCZ** in solutions and the solid state.

Luminogen	solvent	[a]$\lambda_{abs,\ solution}$	[b]$\lambda_{abs,solid}$	[c]$QY_{solution}$	[d]$\lambda_{FL,solution}$	[e]$\lambda_{FL,solid}$	[f]QY_{solid}
NIBBCZ	Benzene	290, 311, 372	410	71.5%	490	478	42.3%
	Toluene	291, 313, 375		77.5%	489		
	EtOAc	290, 307, 368		43.4%	544		
	DCM	292, 308, 366		44.0%	554		
	THF	292, 309, 371		52.3%	546		
NIFBCZ	Benzene	324, 341, 373	411	76.9%	489	510	62.4%
	Toluene	324, 341, 373		75.2%	492		
	EtOAc	315, 338, 369		58.3%	538		
	DCM	316, 341, 366		55.8%	556		
	THF	317, 338, 369		62.7%	542		

[a]Solution absorption peak in nm (10 μM), [b]Solid absorption peak in nm, [c]Quantum yield (QY) in solutions, [d]Solution fluorescence (FL) peak in nm (10 μM), [e]Solution fluorescence (FL) peak, [f]Quantum yield (QY) in the solid state. EtOAc is ethyl acetate, DCM is dichloromethane, THF is tetrahydrofuran

Table S2 Summary of crystallographic data and structure refinement details for **NIBBCZ** and **NIFBCZ.**

Identification code	**NIBBCZ**	**NIFBCZ**
Empirical formula	$C_{61}H_{44}N_4O_2$	$C_{61}H_{42}N_4O_2$
Formula weight	865.00	862.98
Temperature	300 K	300 K
Wavelength	1.54178 Å	1.54178 Å
Crystal system	triclinic	triclinic
Space group	*P-1*	*P-1*
a	9.7156(2) Å	10.5631(2) Å
b	14.4139(4) Å	13.1305(3) Å
c	18.4817(5) Å	20.4346(4) Å
α	101.252(2)°	101.7950(10)°
β	99.0150(10)°	97.3960(10)°
γ	108.7820(10)°	110.1730(10)°
Volume	2335.13(10) $Å^3$	2542.27(9) $Å^3$
Z, Calculated density	2,1.230 mg m^{-3}	2, 1.127 mg m^{-3}
Absorption coefficient	0.583 mm^{-1}	0.536 mm^{-1}
2θ range for data collection	5.018 to 136.726°	4.524 to 137.102°
Index ranges	$-11 \le h \le 11$ $-17 \le k \le 17$ $-22 \le l \le 22$	$-12 \le h \le 12$ $-15 \le k \le 14$ $-24 \le l \le 24$
Reflections collected	79601	89102
Independent reflections	8575 [Rint = 0.0716, Rsigma = 0.0361]	9360 [Rint = 0.1021, Rsigma = 0.0456]
Data/restraints/parameters	8575/1/605	9360/0/605
Goodness-of-fit on F^2	1.041	0.973
Final *R* indices [$I > 2\sigma(I)$]	$R_1 = 0.0810$ $wR_2 = 0.2243$	$R_1 = 0.0613$ $wR_2 = 0.1556$
Final *R* indices (all data)	$R_1 = 0.0946$ $wR_2 = 0.2360$	$R_1 = 0.0993$ $wR_2 = 0.1877$

Table S3 Selected interaction patterns in the Crystals of **NIFBCZ** and **NIBBCZ**.

	interaction	color	d (Å)	interaction	color	d (Å)
NIFBCZ	C_4-H_4···π	red	2.812	C_{48}-H_{48}···π	green	2.778
	C_9-H_9···π	orange	2.750	C_{47}-H_{47}···π	blue	2.659
	C_{16}-H_{16}···π	yellow	2.700	C_{41}-H_{41}···π	violet	2.774
NIBBCZ	C_1-H_1···π	red	3.302	C_{41}-H_{41}···π	green	2.784
	C_{15}-H_{15}···π	orange	2.852	C_{48}-H_{48}···N_3	yellow	2.701
	C_{14}-H_{14}···π	violet	2.680	C_{47}-H_{47}···O_1	blue	2.634

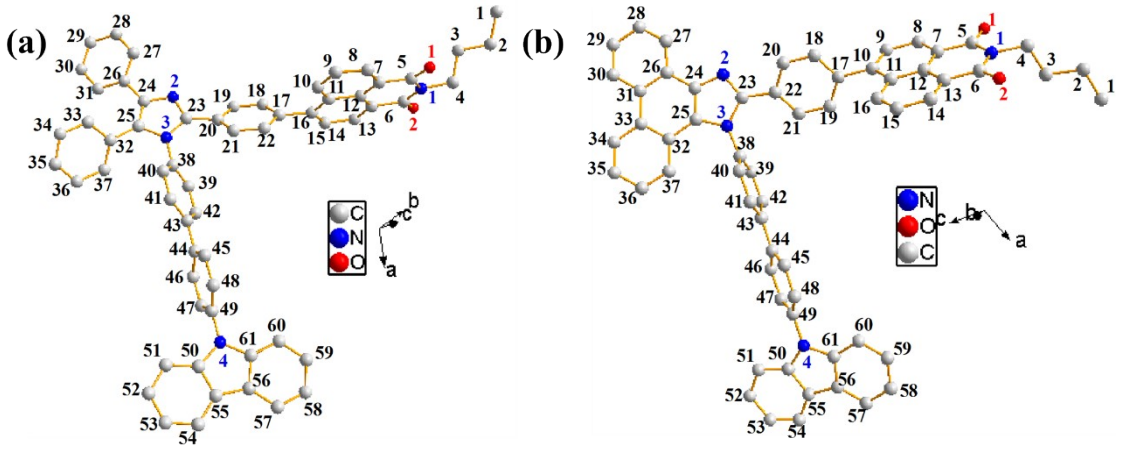

Fig. S2 The molecular structures of (a) **NIFBCZ** and (b) **NIBBCZ** obtained from single crystal x-ray diffraction. The hydrogen atoms are omitted for clarity.

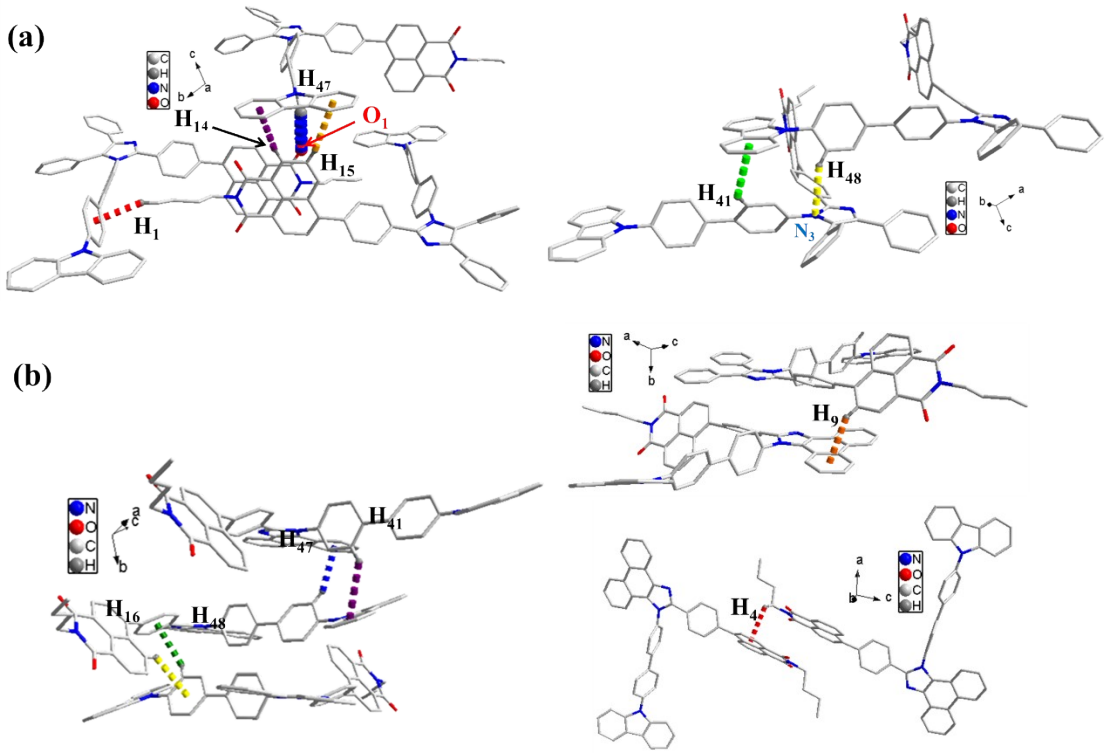

Fig. S3 Packing diagram showing weak intermolecular interactions between adjacent molecules, including (a) C-H_{48}⋯ N_3 hydrogen bond (yellow), C-H_{47}⋯ O_1 hydrogen bond (blue), and C-H⋯π weak interactions (dashed lines in red, orange, and green colors) in **NIBBCZ** and (b) C-H⋯π weak interactions (dashed lines in red, orange, yellow, green, blue, and violet colors) in **NIFBCZ**.

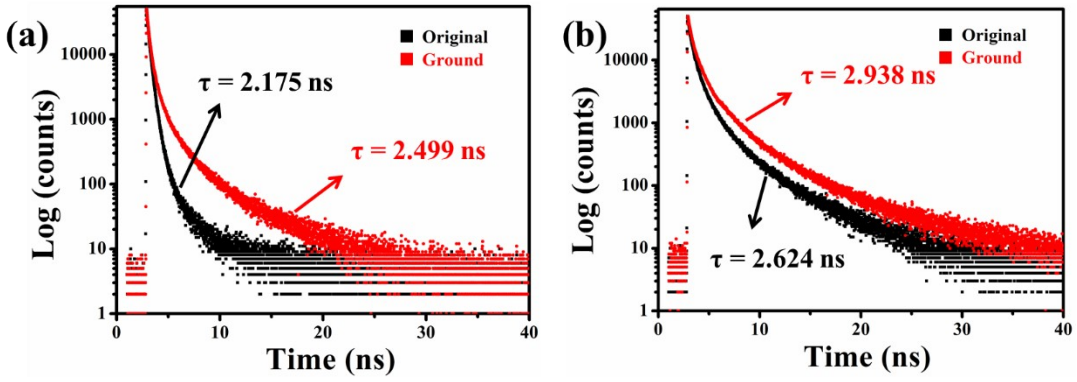

Fig. S4 Emission lifetime of (a) **NIBBCZ** and (b) **NIFBCZ** in original and ground samples.

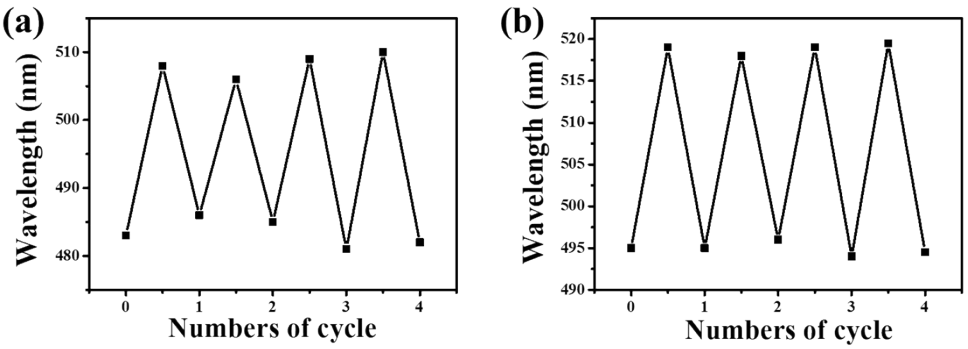

Fig. S5 Maximum peak of ground and fumed (a) **NIBBCZ** and (b) **NIFBCZ** in 5-cycle treatment.

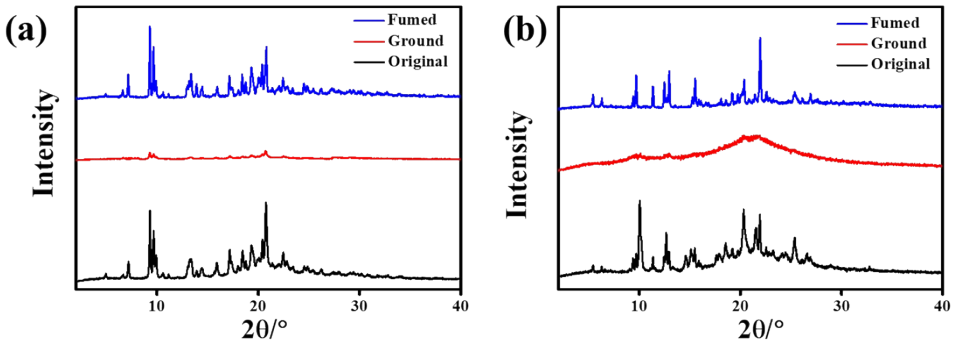

Fig. S6 PXRD patterns of pristine, ground, and fumed samples of (a) **NIBBCZ** and (b) **NIFBCZ**.

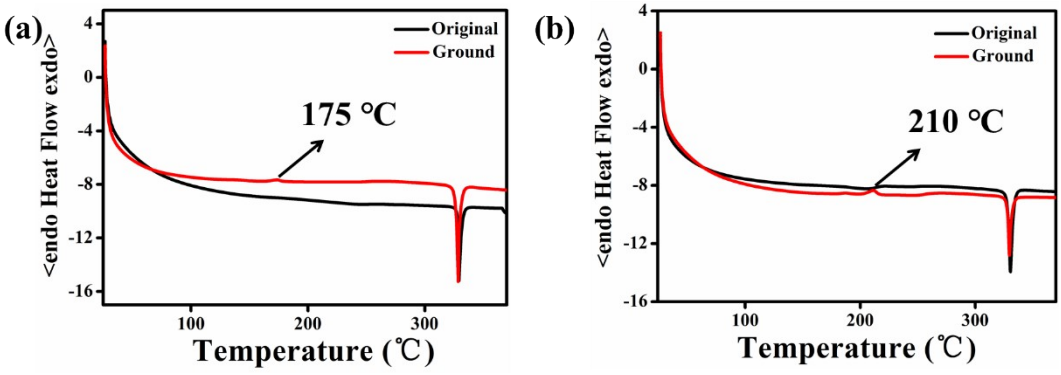

Fig. S7 DSC curves of (a) **NIBBCZ** and (b) **NIFBCZ** in the original and ground samples (Scan rate: 10 °C/min).

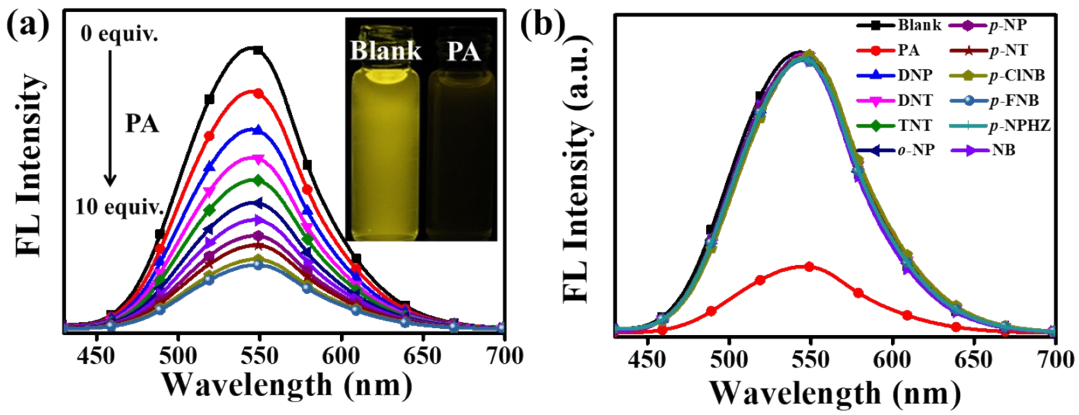

Fig. S8 (a) Emission spectrum of **NIBBCZ** in the absence and presence of varying concentration of PA. (b) Emission spectra of **NIBBCZ** in the absence and presence of different NACs (10 equiv.). DNP is 2,4-dinitrophenol, DNT is 2,4-dinitro toluene, TNT is trinitrotoluene, *o*-NP is *o*-nitrophenol, *p*-NP is *p*- nitrophenol, *p*-NT is *p*-nitrosotoluene, *p*-ClNB is *p*-chloronitrobenzene, *p*-FNB is *p*-fluoronitrobenzene, *p*-NPHZ is *p*-nitrophenylhydrazine, NB is nitrobenzene.

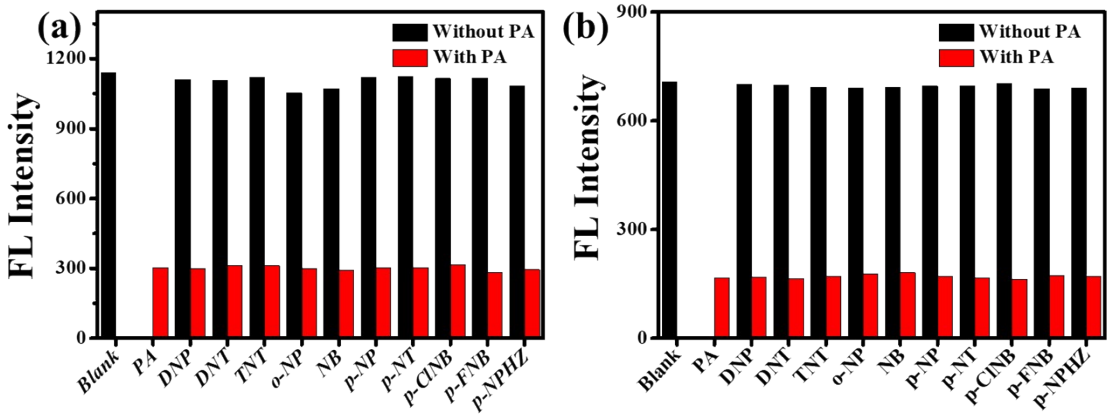

Fig. S9 The fluorescence changes after adding NACs (black) and then adding PA (red) to the mixed solution of (a) **NIFBCZ** and (b) **NIBBCZ**.

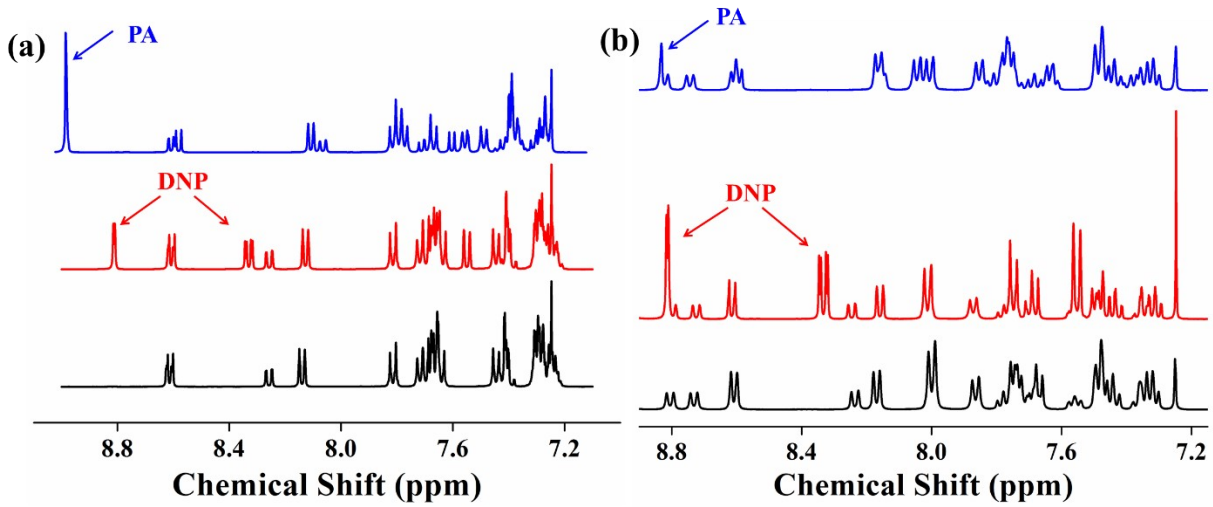

Fig. S10 ^{1}H NMR spectra of (a) **NIBBCZ** and (b) **NIFBCZ** before and after PA and DNP titration at room temperature.

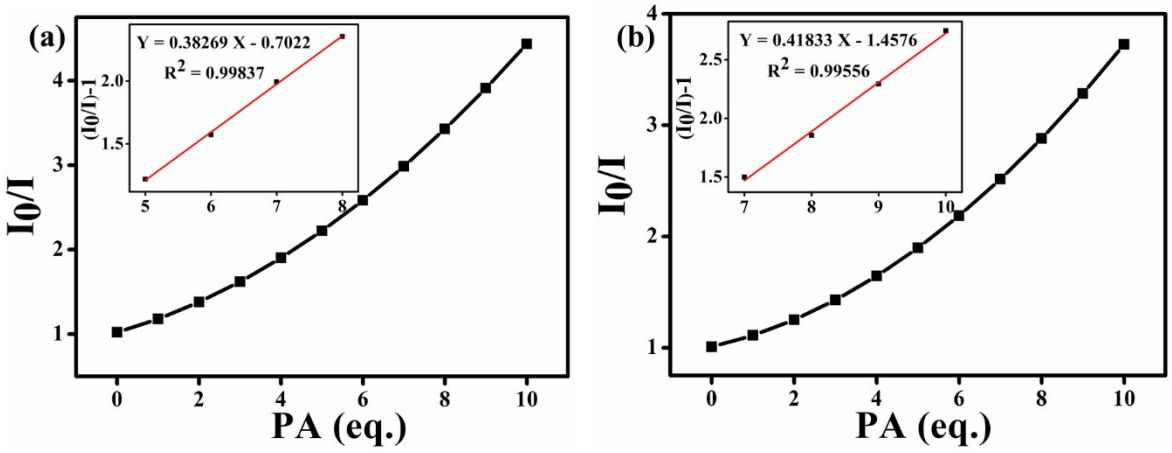

Fig. S11 Stern-Volmer plots of (a) **NIBBCZ** and (b) **NIFBCZ**.

Table S4 A comparison of picric acid detection of our work with the results collected from the reported literature.

Materials	Response mode	Detection method	LOD (nM)	Ref.
Polyfluorene derivative (PCFSe)	Turn-off	Fluorescence	270	S2

Poly(allylamine) hydrochloride (PAH)	Turn-off	Fluorescence	79	S3
pyranone based Schiff base (DFA)	Ratiometric	Fluorescence	692	S4
Coumarin-encapsulated MOF (C-CAU-10)	Turn-off	Fluorescence	1000	S5
Fe_2O_3-CdSe nanocomposite	Turn-off	Fluorescence	2200	S6
Benzimidazole acrylonitriles	Ratiometric	Fluorescence	10000	S7
Nanomaterials of naphthalene monoimide	Turn-off	Fluorescence	149	S8
Polyvinylpyrrolidone templated copper Nanoclusters (PVP-CuNCs)	Turn-off	Fluorescence	840	S9
Tetraphenylethylene arylimidazole derivatives	Turn-off	Fluorescence	564	S10
Diflfluoroboron derivatives	Turn-off	Fluorescence	497	S11
Arylimidazole Derivatives (NIBBCZ)	Turn-off	Fluorescence	**97**	**This work**

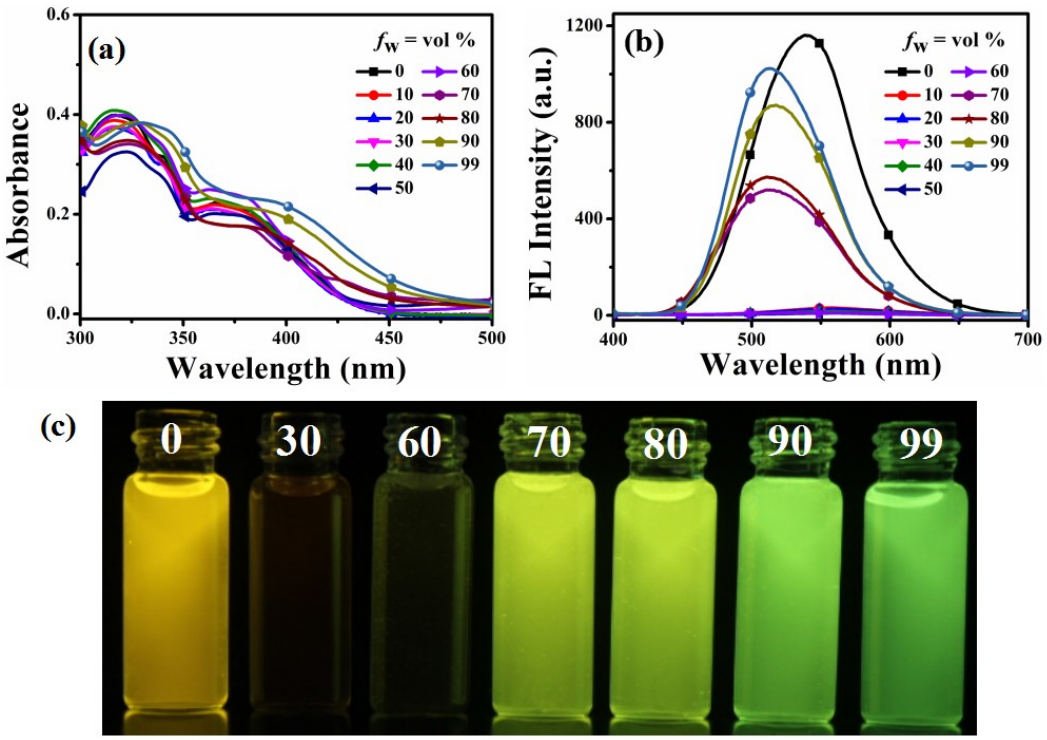

Fig. S12 (a) UV-vis and (b) FL spectra of **NIFBCZ** in THF/H_2O mixtures with different water fractions (f_w). (c) Photographs of **NIFBCZ** in the solvent mixture with different water fractions (v/v, %) labeled on the bottleneck under 365 nm UV irradiation.

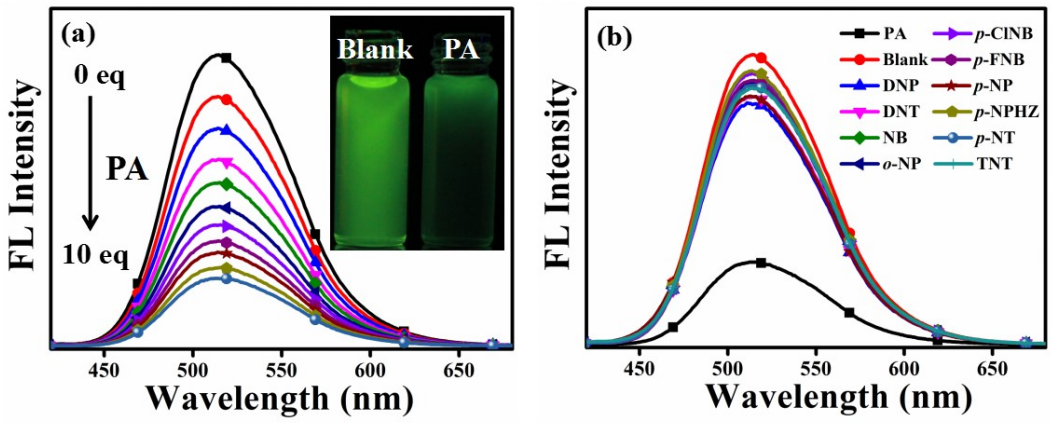

Fig. S13 (a) Fluorescence spectra of adding different PA equivalents to H_2O/THF (f_w = 99%) of **NIFBCZ**. Inset shows the photographs of **NIFBCZ** in the absence and presence of PA under 365 nm UV irradiation. (b) The fluorescence spectra obtained of **NIFBCZ** in H_2O/THF mixture (f_w = 99%) upon addition of different NACs (10 equiv.). DNP is 2,4-dinitrophenol, DNT is 2,4-dinitro toluene, TNT is trinitrotoluene, *o*-NP is *o*-nitrophenol, *p*-NP is *p*- nitrophenol, *p*-NT is *p*-nitrosotoluene, *p*-ClNB is *p*-chloronitrobenzene, *p*-FNB is *p*-fluoronitrobenzene, *p*-NPHZ is *p*-nitrophenylhydrazine, NB is nitrobenzene.

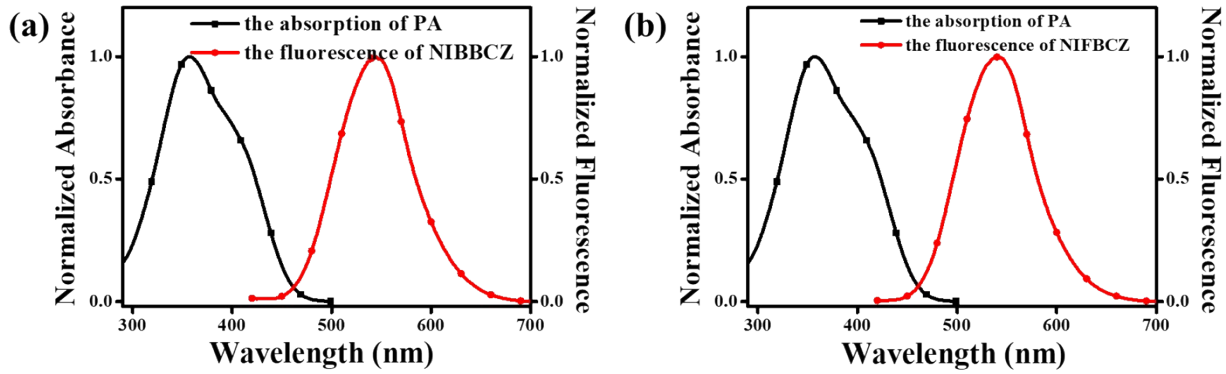

Fig. S14 Normalized absorption spectrum of PA and normalized emission spectrum of (a) **NIBBCZ** and (b) **NIBBCZ** in THF solutions, 10 μM, 25 °C.

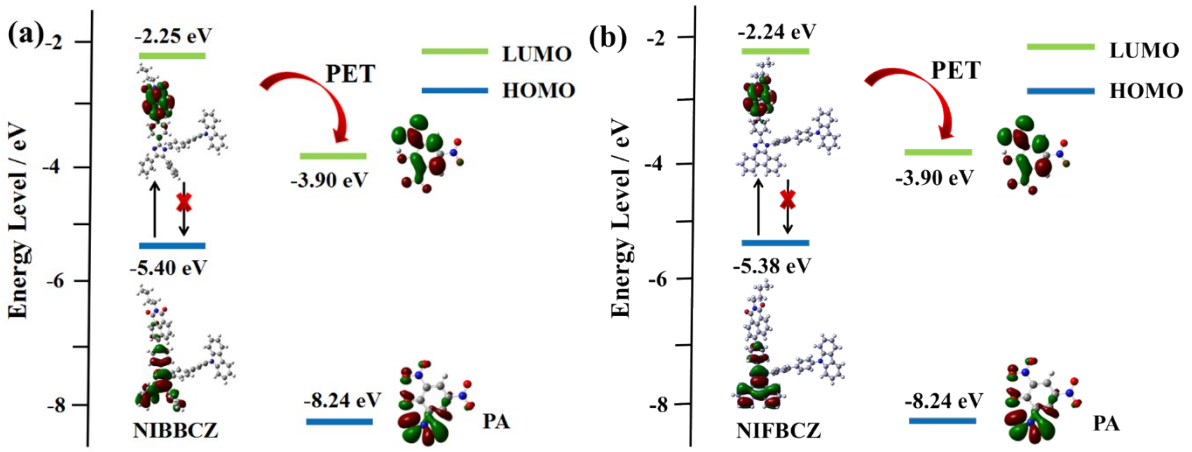

Fig. S15 HOMO and LUMO energy levels of (a) **NIBBCZ** and (b) **NIFBCZ** and PA.

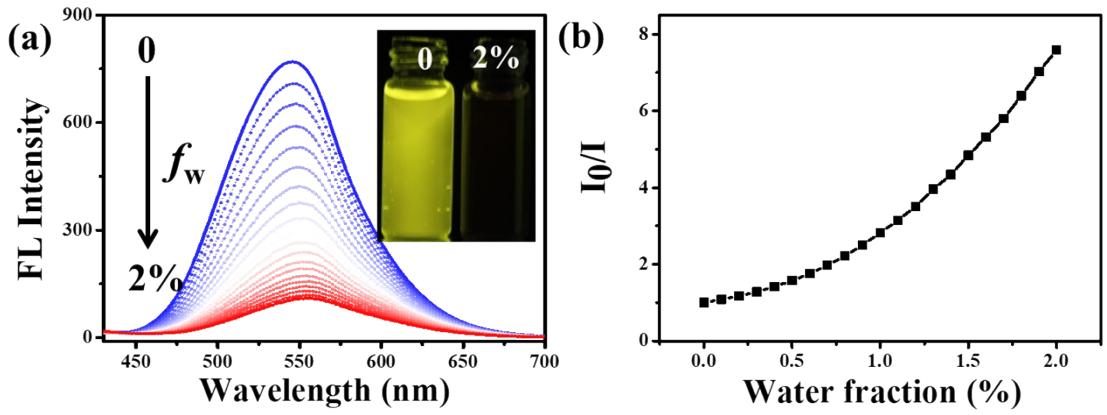

Fig. S16 (a) Fluorescence spectra of **NIBBCZ** in THF containing trace water. Insert shows photograph under UV lamp at 365 nm before and after water added. (b) The Stern-Volmer plot of the emission intensity of **NIBBCZ** against water fraction.

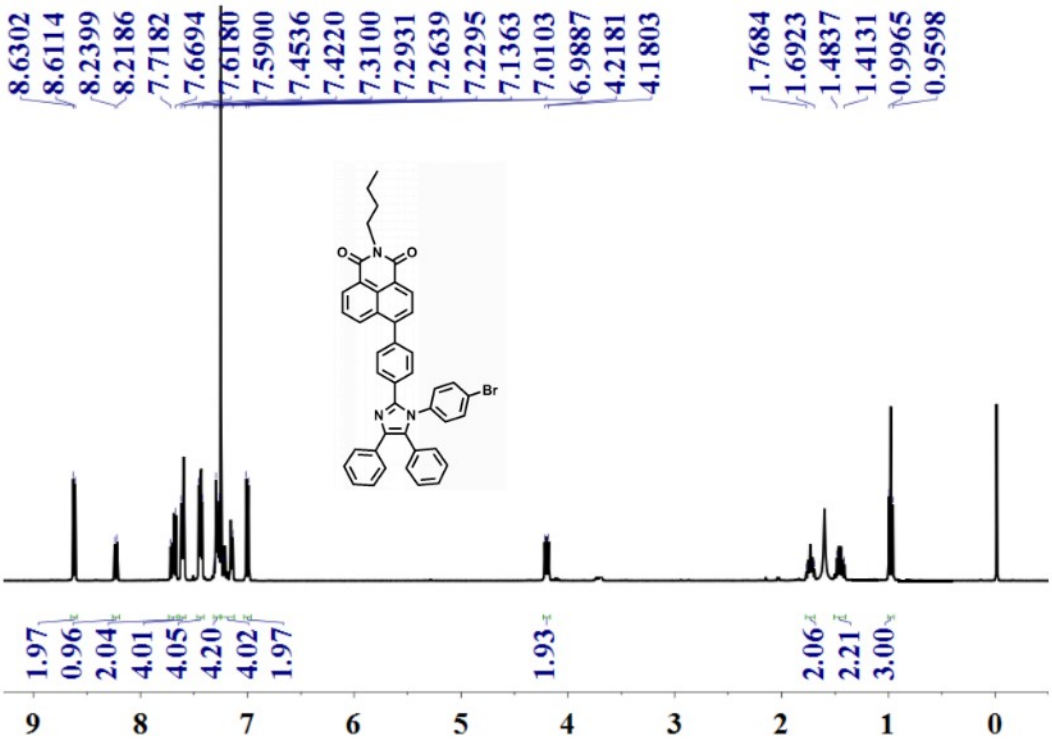

Fig. S17 ^{1}H NMR spectrum of **NIBBr** in $CDCl_3$.

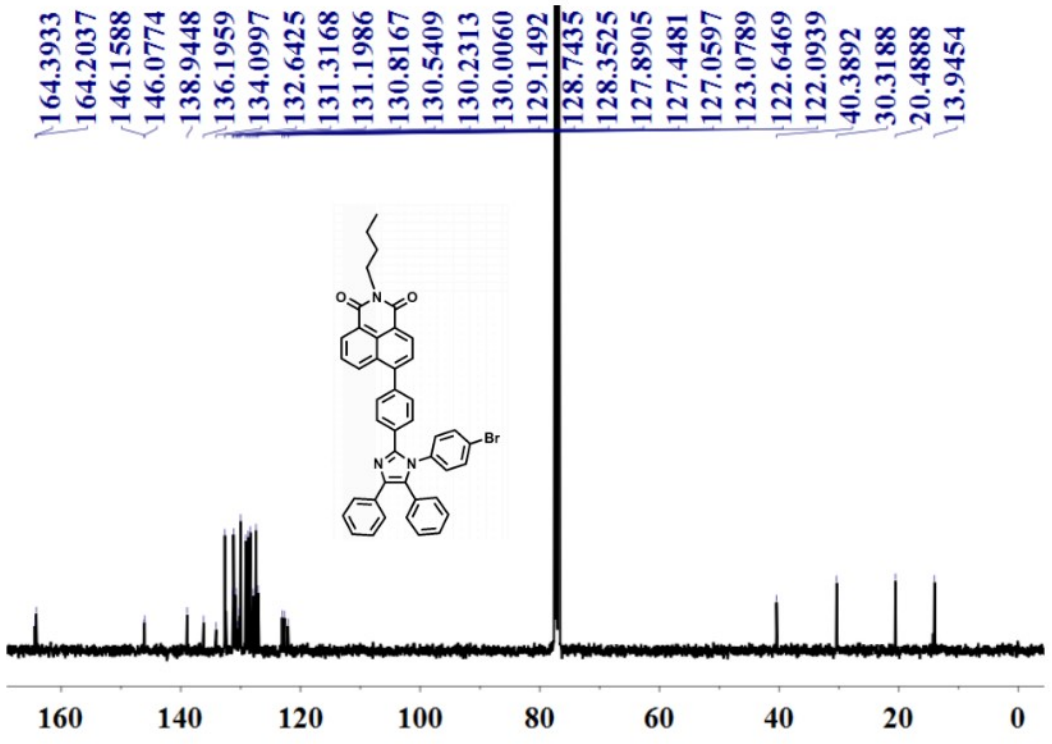

Fig. S18 ^{13}C NMR spectrum of **NIBBr** in $CDCl_3$.

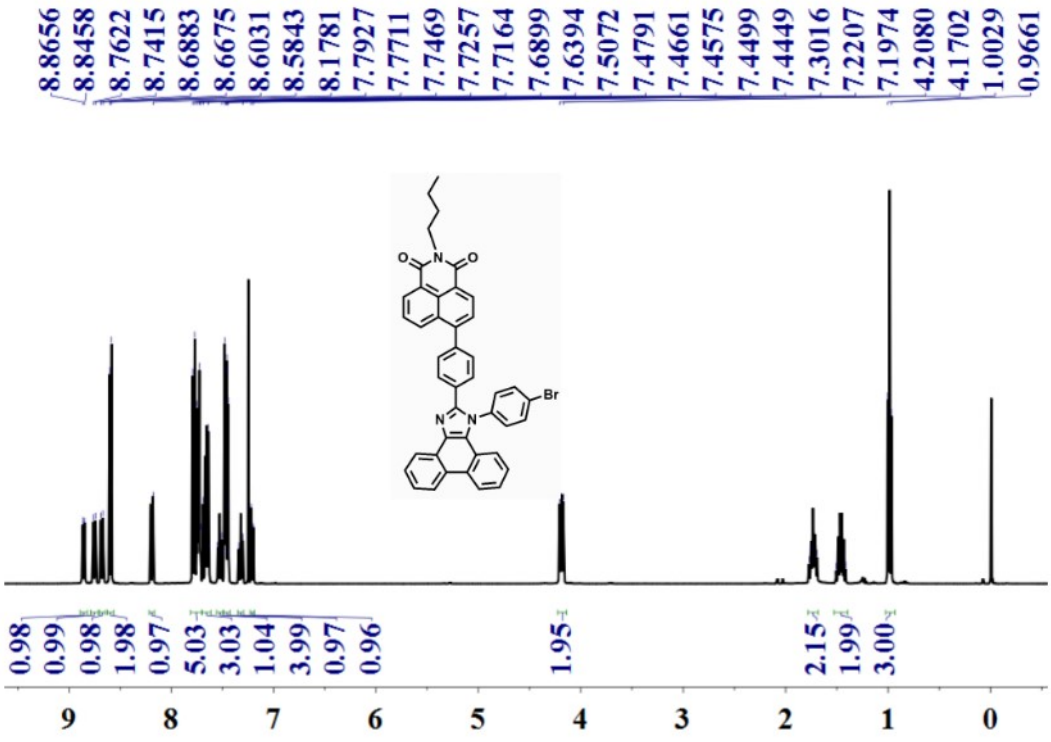

Fig. S19 ^{1}H NMR spectrum of **NIFBr** in $CDCl_3$.

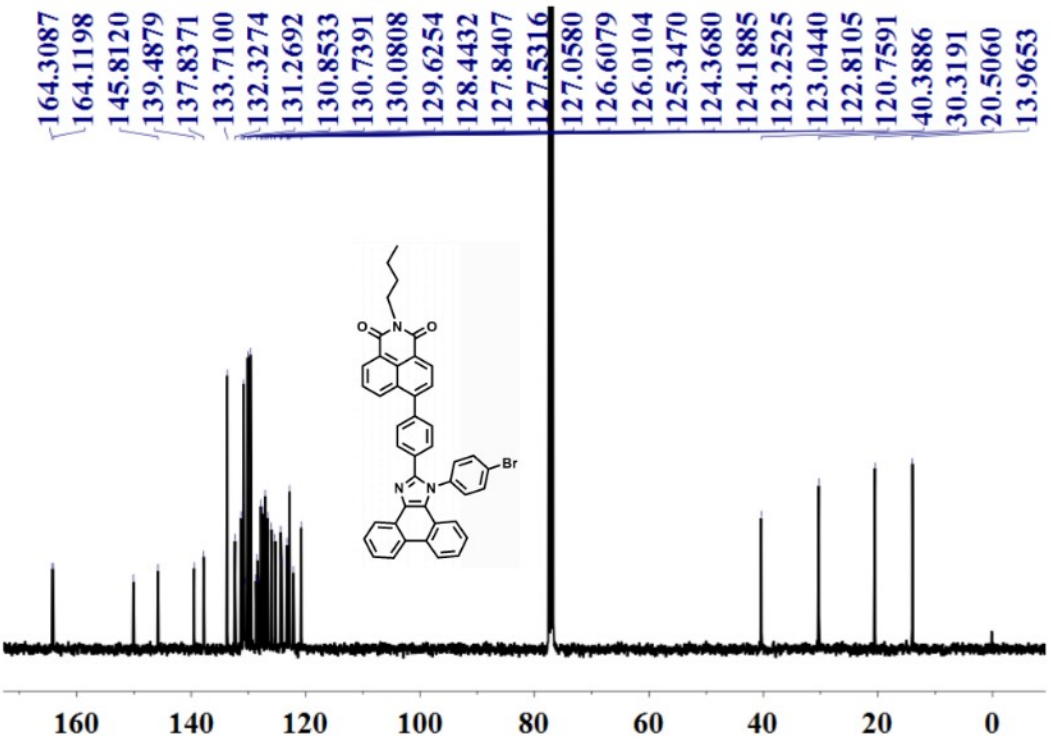

Fig. S20 ^{13}C NMR spectrum of **NIFBr** in $CDCl_3$.

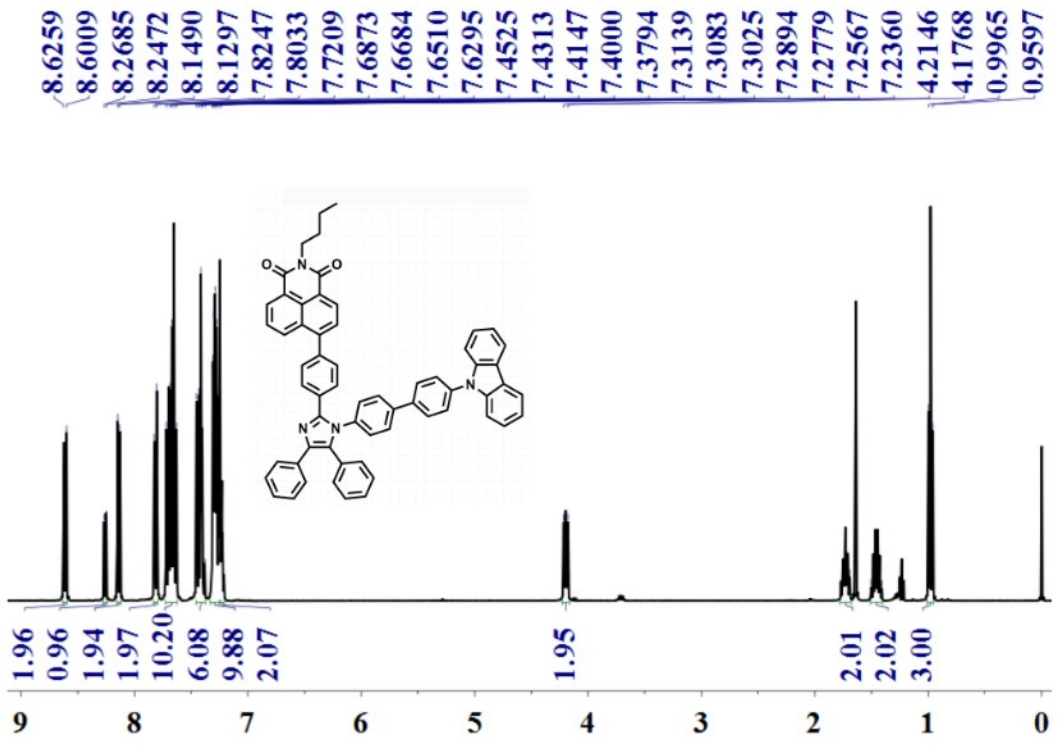

Fig. S21 ^{1}H NMR spectrum of **NIBBCZ** in $CDCl_3$.

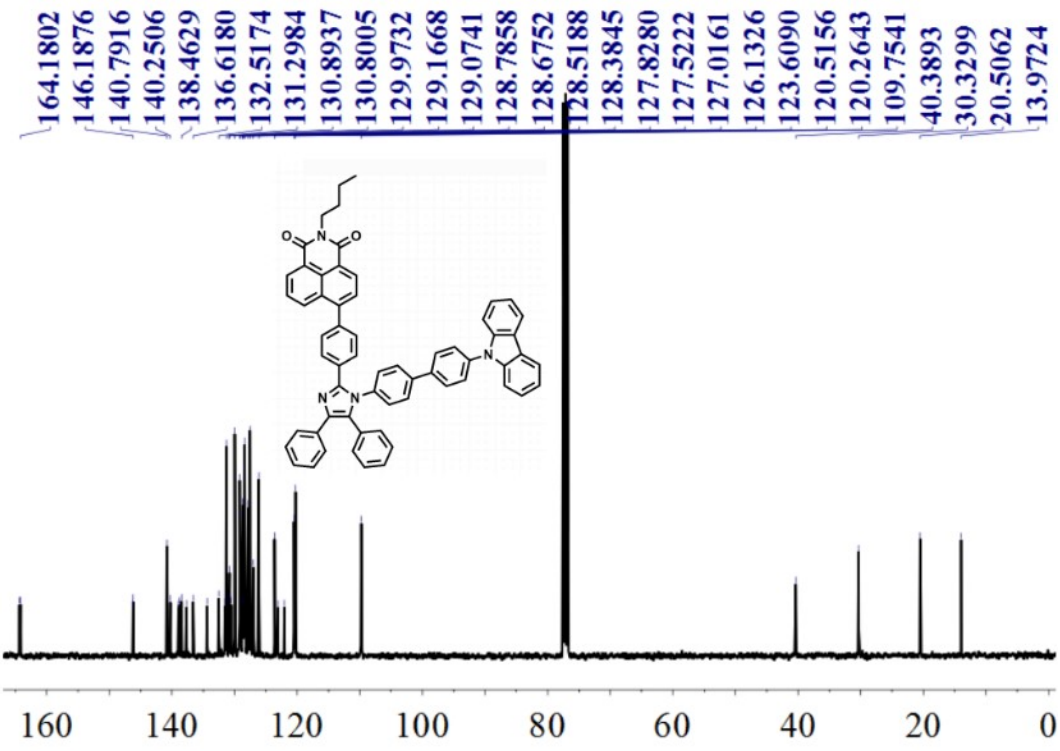

Fig. S22 ^{13}C NMR spectrum of **NIBBCZ** in $CDCl_3$.

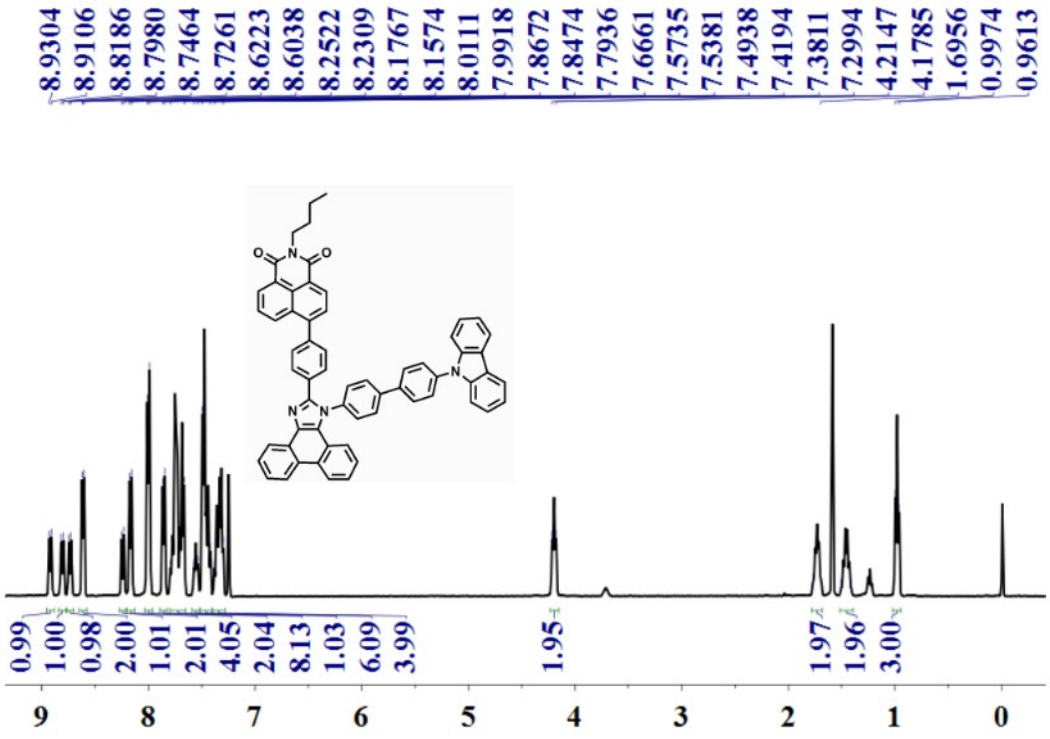

Fig. S23 ^{1}H NMR spectrum of **NIFBCZ** in $CDCl_3$.

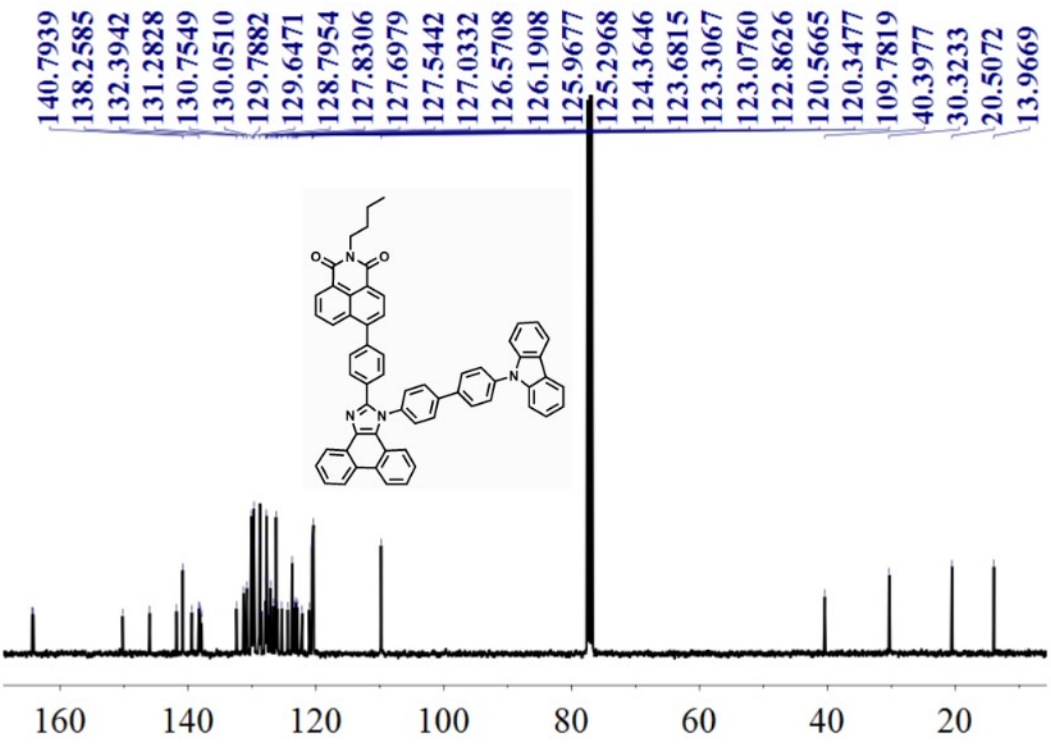

Fig. S24 ^{13}C NMR spectrum of **NIFBCZ** in $CDCl_3$.

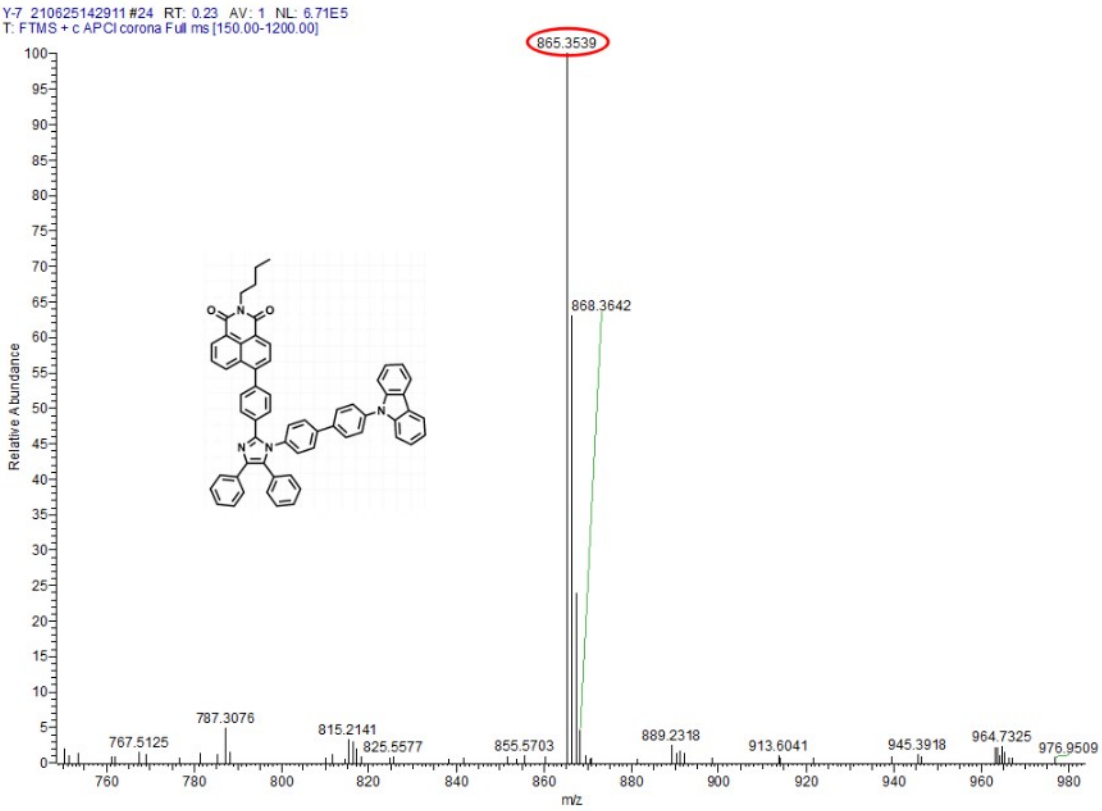

Fig. S25 HR-MS spectrum of **NIBBCZ** in CH_2Cl_2.

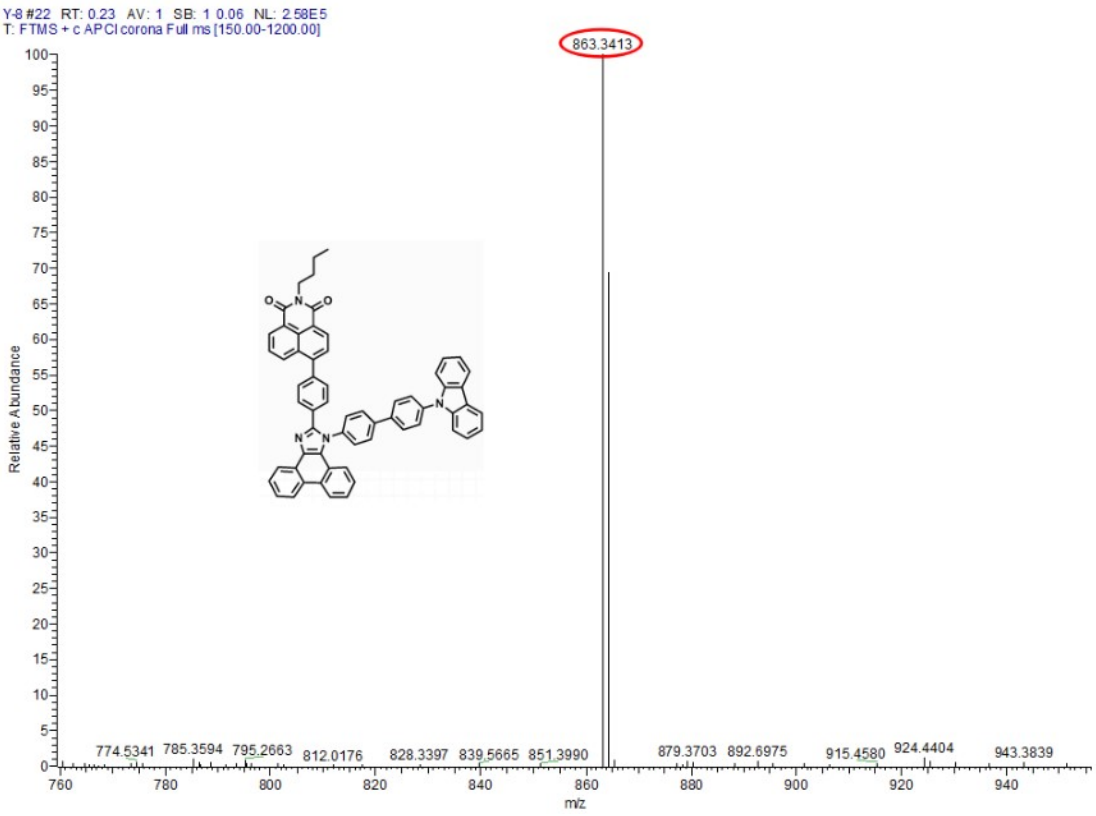

Fig. S26 HR-MS spectrum of **NIFBCZ** in CH_2Cl_2.

Reference:

[S1] M. R. Li, F. K. Du, P. Xue, X. C. Tan, S. G. Liu, Y. Zhou, J. Chen, L. J. Bai, An AIE fluorescent probe with a naphthalimide derivative and its application for detection of hypochlorite and imaging inside living cells, *Spectrochim. Acta A Mol. Biomol. Spectrosc.*, 2020, **227**, 117760.

[S2] W. Zhang, B. Gao, X. Guo, W. Dong, Polyfluorene based fluorescent sensor for sensitive and selective detection of picric acid, *Mater. Lett.*, 2022, **306**, 130860.

[S3] S. Kaja, D.-P. Damera, A. Nag, A metal-enhanced fluorescence sensing platform for selective detection of picric acid in aqueous medium, *Anal. Chim. Acta*, 2020, **1129**, 12-23.

[S4] A. Goel, R. Malhotra, Efficient detection of Picric acid by pyranone based Schiff base as a chemosensor, *J. Mol. Struct.*, 2022, **1249**, 131619.

[S5] B. Jiang, W. Liu, S. Liu, W. Liu, Coumarin-encapsulated MOF luminescence sensor for detection of picric acid in water environment, *Dyes Pigm.*, 2021, **184**, 108794.

[S6] V. Kumar, A. Kumar, M.-K. Chini, S. Satapathi, Fluorescent Fe_2O_3-CdSe nanocomposite probe for selective detection and removal of picric acid, *Mater. Chem. Phys.*, 2021, **260**, 124130.

[S7] P. Jana, M. Yadav, T. Kumar, S. Kanvah, Benzimidazole-acrylonitriles as chemosensors for picric acid detection, *J. Photoch. Photobio. A*, 2021, **404**, 112874.

[S8] S. Dey, A. Saha, P. Kumar, C. Kar, S. Chakraborty, P.-K. Sukul, Self-assembled nanomaterials of naphthalene monoimide in aqueous medium for multimodal detection of picric acid, *J. Photoch. Photobio. A*, 2022, **423**, 113599.

[S9] Q. Lin, H. Chu, J. Chen, L. Gao, W. Zong, S. Han, J. Li, Dual-emission ratiometric fluorescence probe based on copper nanoclusters for the detection of rutin and picric acid, *Spectrochim. Acta A Mol. Biomol. Spectrosc.*, 2022, **270**, 120829.

[S10] S. Guo, G. Zhang, F. Chen, Y. Ni, J. Huang, L. Kong, J. Yang, Multi-stimuli responsive properties and structure–property studies of tetraphenylethylene functionalized arylimidazole derivatives, *New J. Chem.*, 2021, **45**, 21327-21333.

[S11] Y. Ni, S. Zhang, X. He, J. Huang, L. Kong, J. Yang, J. Yang, Dual-state emission difluoroboron derivatives for selective detection of picric acid and reversible acid/base fluorescence switching, *Anal. Method*s, 2021, **13**, 2830-2835.